Ion erosion induced nanogrooves: temporal evolution and azimuth dependence

2009 J. Phys.: Condens. Matter 21 224002

(http://iopscience.iop.org/0953-8984/21/22/224002)

J. Phys.: Condens. Matter **21** (2009) 224002 (12pp) doi:10.1088/0953-8984/21/22/224002

Ion erosion induced nanogrooves: temporal evolution and azimuth dependence

Herbert Wormeester and Bene Poelsema

Solid State Physics, MESA + Institute for Nanotechnology, University of Twente, Enschede, The Netherlands

E-mail: h.wormeester@utwente.nl

Received 8 January 2009, in final form 14 January 2009
Published 12 May 2009
Online at stacks.iop.org/JPhysCM/21/224002

Abstract

Ion sputtering at grazing incidence of the Cu(001) surface leads to the formation of a regular pattern of nanogrooves with a well defined separation distance between the grooves. The grooves are only two atomic layers deep for a low ion flux and their height remains the same independent of sputter time. The average separation distance of the nanogrooves is at least 5 nm and can be increased beyond 40 nm, depending on substrate temperature, fluence, the ion's mass and energy. Anneal experiments of a nanogroove pattern also show an increase in average nanogroove separation with anneal time. The increase of the average nanogroove separation with time is larger for nanogrooves created along a ⟨100⟩ azimuth compared to the ⟨110⟩ azimuth. The ⟨100⟩ oriented step edges show a high density of kinks, suggesting that detachment from kinks is the rate limiting step in the process that governs the periodicity. Also both adatoms and vacancies are involved in this process, while the grazing incident ion beam continuously creates new nanogrooves. The creation of new nanogrooves and the movement observed during annealing are used as ingredients for a description of the temporal behaviour of the average nanogroove periodicity.

(Some figures in this article are in colour only in the electronic version)

1. Introduction

Controlled ion bombardment provides an efficient route for the creation of periodic nanostructures on macroscopic surfaces. First reports of the formation of a ripple pattern with nanometre dimension upon ion bombardment were made some 50 years ago [1]. A breakthrough in understanding the created ripple patterns was the continuum theory of Bradley and Harper [2] (BH). This theory describes the height evolution of the surface in terms of competing processes. The ion beam induces a height instability as the result of a heterogeneous sputter efficiency on a rough surface, according to Sigmund's theory on the ion impact on a corrugated surface [3]. This heterogeneous roughening is countered by thermally activated diffusion processes. Mullins was the first who extensively studied the coarsening of rough surfaces [4, 5]. BH showed that the combination of these two effects explains the experimentally observed ripple pattern and moreover also explained the experimentally observed phenomenon of a critical angle. For ion incidence angles between normal incidence and the critical angle, the BH theory predicts a ripple pattern with ripples running perpendicular to the plane of incidence of the ion beam. For more oblique incidence the ripples should be oriented in the direction of the ion beam, in accordance with experimental observations. The distance between ripples is also obtained from this theory and is determined by the ratio of the diffusion rate and the sputter rate. The continuum description has been extensively modified by especially Barabási, Cuerno and co-workers [6–8] in order to explain experimental observations like the saturation of both the ripple amplitude and periodicity. The ion beam induced ripples were shown to occur in many different materials, ranging from oxides to crystalline metals, and their periodicity can be set between 100 and 1000 nm. The kinetics of ripple formation on Cu(001) were studied by Chason *et al* [9]. Their experiments showed the influence of temperature, ion flux and

azimuthal orientation of the crystal on the amplitude and the periodicity of the created ripples at elevated temperatures. The observed coarsening was attributed to attachment–detachment limited kinetics. This work focuses strongly on the difference between the BH regime, the regime in which energy barriers for interlayer mass transport play a role and the regime in which no nanopatterning takes place. The borders between these three regimes are at rather high temperature, showing ripples with a periodicity of several hundred nanometres. In a review article, Chan and Chason [10] introduced a kinetic phase diagram showing the various regions of nanopatterning on Cu(001) and Ag(001) surfaces for oblique incidence ion beam patterning. In this they also provide an overview of related experimental and theoretical work, including the work on bombarding a Cu or Ag substrate at temperatures below 350 K. At these temperatures ripples with a much smaller characteristic length scale are observed as reported by the Valbusa group [11–14] and for Cu(001) by van Dijken *et al* [15, 16]. The ripples on both the Cu and Ag(110) surfaces were analysed in terms of the continuum equation introduced by BH. This theory explained the observed dependence of the ripple orientation on both the polar and azimuthal ion incidence angles. However, not only the ripple amplitude, but also the periodicity of the ripples, was found to change with sputter time. This change of periodicity is beyond the original analysis of the BH equation [17]. The coarsening of such ripples on Ag(110) was studied to observe the temporal behaviour of the amplitude of 1D ripples limited by detachment kinetics [18]. Kim *et al* [19] studied the influence of ion bombardment on the Pd(001) surface and used the extended Kuramoto–Sivashinsky model to explain their results. Recently, we reported on the temporal behaviour of a ripple pattern created by ion sputtering with a polar angle of incidence of 70° on a Ag(001) surface at temperatures around 400 K [20]. This behaviour is very different from that observed at low temperatures [14]. A comparison with the theoretical results of Cuerno and co-workers [21] suggests that the mechanism behind the observed temporal behaviour should involve a very efficient coarsening mechanism.

The nanopatterning of a Cu or Ag(001) surface at grazing incidence is markedly different from that at a polar angle of incidence of 70° [15, 16]. The impingement of the ions at an angle with the surface normal larger than the critical angle for sputtering [22] leads to an ion erosion process that is very different from that used in the continuum theory for sputtering, i.e. in Sigmund's sputter model [3]. This is directly evident from the much lower sputter yield on a pristine surface. Most ions are approximately specularly reflected from the surface without significant energy transfer, and only a small fraction of the incident ions is actually involved in an erosive process. On the other hand a very high sputter yield is observed at grazing incidence if an ion approaches the surface just in front of an ascending step edge. This geometry leads to a very efficient impact of the ion as discussed in [16] and shown with STM by Hansen *et al* [23]. The ripple patterns that are the result of the grazing incidence ion bombardment were called nanogrooves. The main reason for this name is that the height variation is very small, i.e., they are only about two atomic layers deep. The average distance between these nanogrooves was shown to depend on temperature and ion energy. More strikingly, it was found that the average distance depends on the azimuthal direction of the incident ion beam. A larger average distance was found for sputtering along the [100] azimuth compared to sputtering along the [110] azimuth for temperatures above 200 K [15]. The temperature dependence of the azimuth related difference in periodicity indicates that this is governed by the diffusion processes on the surface. Especially the interlayer mass transport is known to depend strongly on the orientation of the step edge. This has been very clearly illustrated by the observed variation in morphology upon sputtering at normal incidence [24]. The highly efficient interlayer mass transport over the ⟨100⟩ oriented step edge compared to the ⟨110⟩ step edge was shown to be responsible for a change in orientation of the etch pyramid at a temperature of 300 K and above.

In this paper we report on a systematic study of ripple formation through mild grazing incidence sputtering of the Cu(001) surface. The observed temporal evolution of these ripples cannot be explained within present continuum models: the ripple amplitude remains similar, while the ripple periodicity increases with sputter time. Sputtering along [100] results in a larger distance between nanogrooves as compared to sputtering along $[1\bar{1}0]$ for a given sputter time at temperatures of 235 K and above. Also a clear saturation of this distance is observed for sputtering along [100]. Coarsening of these nanogrooves points to detachment processes that are responsible for the increase of the periodicity of the ion induced pattern with time.

2. Experimental details

The periodic morphology on the Cu(001) surface after ion bombardment is characterized with high-resolution low-energy electron diffraction (HR-LEED). The Omicron (SPA-LEED) instrument used for this has a resolution of ∼0.1% of the Brillouin zone (BZ). All experiments were conducted in ultra-high vacuum (pressure $<10^{-10}$ mbar). After mounting the crystal, the surface was cleaned by several sputter–anneal cycles and the cleanliness of the surface was checked with Auger electron spectroscopy. After the impurities were below the detection limit of Auger, a subsequent sputtering at 800 K was performed until the FWHM of the (0, 0) beam measured with HR-LEED was ∼0.3–0.4% BZ. This corresponds to an average terrace starting width of about 80 nm. The Cu(001) surface was prepared anew before each experiment by 30 min of 800 eV Ar^+ ion sputtering and subsequent annealing up to 800 K for 5 min.

Ion induced patterns were obtained by sputtering with an Ar^+ ion beam of 800 eV. The ion flux reported throughout this paper is the current density measured with a Faraday cup at normal incidence. We did not correct for the influence of the polar angle of incidence on the current density or the sputter yield. Immediately after switching off the etching ion beam, the substrate temperature was quenched to about 100 K to minimize possible disturbing annealing effects [24].

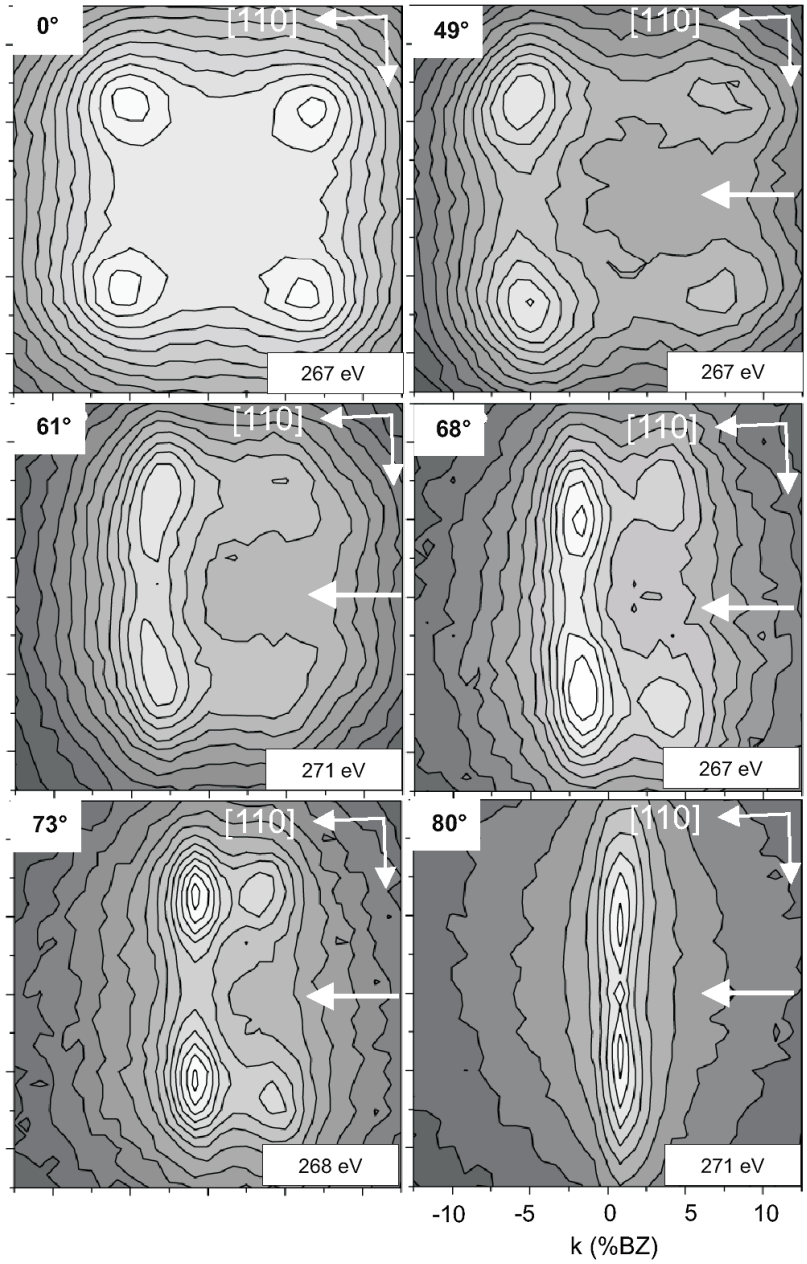

Figure 1. Diffraction profiles around the specular reflected electron beam after oblique incidence Ar^+ ion bombarding a Cu(001) surface for 2 h at 235 K. The polar angle of incidence is indicated and runs from 0° to 80°. The peak profiles were obtained at the electron energies indicated. For the oblique incidence images, the ions impinge from right to left (white arrows). The ion current was 2.2×10^{12} ions cm^{-2} s^{-1}, measured at normal incidence.

3. Influence of the polar and azimuthal angle of incidence

The influence of the polar angle of incidence of an ion beam on the morphology of the surface after substantial erosion is depicted in figure 1. The substrate temperature was 235 K and all surfaces were exposed for 2 h to an incident ion beam with an ion current of 2.2×10^{12} ions cm^{-2} s^{-1}, measured at normal incidence. The erosion at normal incidence leads to the formation of a fourfold symmetric diffraction pattern. The analysis of this pattern showed that etch pyramids are formed with step edges oriented along the ⟨100⟩ azimuth [24]. The fourfold symmetry observed after ion bombardment at normal incidence is broken for oblique incidence sputtering. Ion etching at a polar angle of incidence of around 50° leads to a substantial intensity reduction of two of the four peaks. The fourfold symmetry of the Cu(001) surface is broken around a polar angle of incidence of around 40° and the orientation of the ion beam now also determines the created morphology. The asymmetry of the diffraction pattern is still present for a polar angle of incidence of 73°. A variation of the electron energy shows that the intensity features observed in the diffraction images up to a polar angle of incidence of 73° are related to well developed facets. A detailed analysis of the orientation of

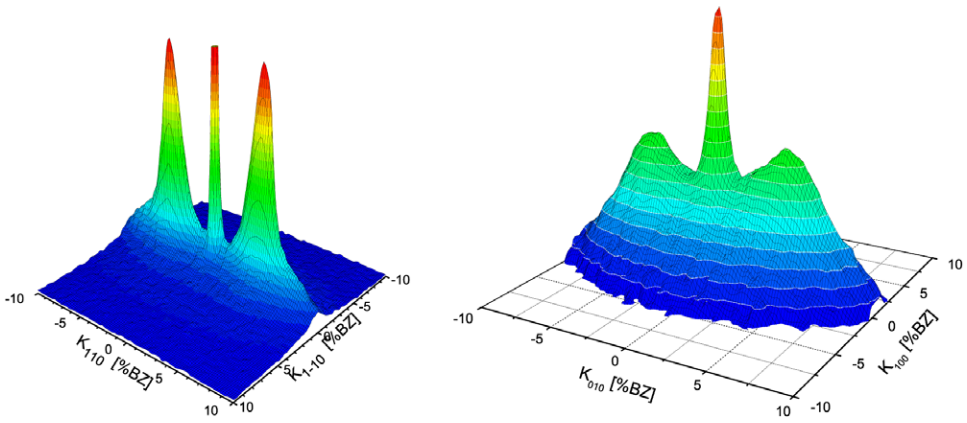

Figure 2. Left, diffraction profile around the specular reflected electron beam after Ar^+ ion bombarding of the Cu(001) surface for 2 h at 235 K along [1$\bar{1}$0] at a polar angle of incidence of 80°. The electron energy was 275 eV and the ion flux was 1.5×10^{12} ions cm^{-2} s^{-1}. Right, diffraction profile around the specularly reflected electron beam after bombarding the Cu(001) surface for 2 h at 235 K along [100]. The electron energy was 275 eV.

these facets shows that the morphology as a result of oblique incidence ion sputtering consists of elongated etch pits. The elongation is in the direction of the ion beam and the facets on the shadow side are much more prominent than those on the illuminated side. The width of the diffraction peak around the in-phase condition is quite narrow for these structures, indicating that they are many atomic layers deep.

Grazing incidence ion bombardment results in a very different pattern. Figure 1 shows that the mirror symmetry is not only present in the plane defined by the incident ion beam. Mirror symmetry in also observed for the plane perpendicular to the ion beam direction. A 3D view of the diffraction profile after ion bombardment at a polar angle of incidence of 80° is shown in the left panel of figure 2. The additional symmetry observed in the diffractogram reflects the creation of a very different morphology on the Cu(001) surface by grazing incident ions. Van Dijken *et al* [15, 16] related this diffraction pattern to the creation of a nanogroove pattern on the surface, with the intensity feature representing the average nanogroove separation. They also observed at a temperature of 250 K an additional feature at twice the periodicity, indicating a highly ordered structure. The relation of the diffraction features to periodic features is verified by an energy dependent line scan along the [110] azimuth as depicted in figure 3(a). In this contour plot, the intensity as a function of the parallel wavevector k_{110} and the perpendicular scattering vector S_z is shown. The scattering factor S_z is defined by $S_z = 2d_{001}/\lambda$, where d_{001} is the spacing between the atomic planes normal to (001) and λ the electron wavelength. The image represents diffraction features around the fifth in-phase scattering condition. The S_z independence of the features at 3.5% BZ clearly shows that they are related to periodic 2D structures at the surface and are not the result of 3D structures or facets. This differs from the diffraction features observed after prolonged grazing incidence sputtering for temperatures above 300 K on Ag(001). The positions of the diffraction features in the BZ change with perpendicular phase, indicating the presence of facets [20].

The diffraction feature in figure 2 shows an approximately Lorentzian line shape in the [110] direction. The position and width of this line shape reflect the average nanogroove separation and distribution of distances between lines. For the quite analogous system of stepped surface with varying terrace width, Wollschläger [25] showed that a Gamma distribution of the separation distances results in a Lorentzian line shape. The key parameters for the Gamma distribution are the average nanogroove separation L and the variation in nanogroove separation σ. From the position of the maximum of the diffracted intensity, we establish an average nanogroove separation of 7.3 nm for the sputter conditions that lead to the image shown in figure 3. The ratio is evaluated as $\sigma/L = 0.5$. The diffraction features show only a very small broadening in the direction of the ion beam compared to a clean surface. This indicates that the etch structures are quite elongated in the direction of the ion beam and that their length is at least similar to the typical distance between terraces on the pristine surface, about 80 nm.

The height of the parallel grooves can be estimated from recording the intensity of the specularly reflected electron beam as a function of S_z. Within the limits of the kinematic approximation, the full width at half maximum (FWHM) of the peak around an integer value of S_z is inversely proportional to the height of the structures on the surface [26, 27]. The relation between the FWHM and the height of a structure was calibrated by measuring the intensity variation with S_z after deposition of half of a monolayer of Cu at 250 K. It is well established that this results in one monolayer high islands, i.e. a system with only two layers exposed [28]. This calibration line is depicted by the solid line in figure 3(b) and gives an FWHM, $\Delta S_z = 0.20$. The FWHM of the intensity variation of the specular beam of the surface after ion bombardment is $\Delta S_z = 0.10$, a reduction by a factor of two. This suggests that only three layers are involved. This height variation is directly related to the line structure created by the ion bombardment as verified by the recording of the intensity variation of the diffraction feature at 3.5% BZ. The FWHM of this diffraction feature is $\Delta S_z = 0.11$, similar to the one obtained for the

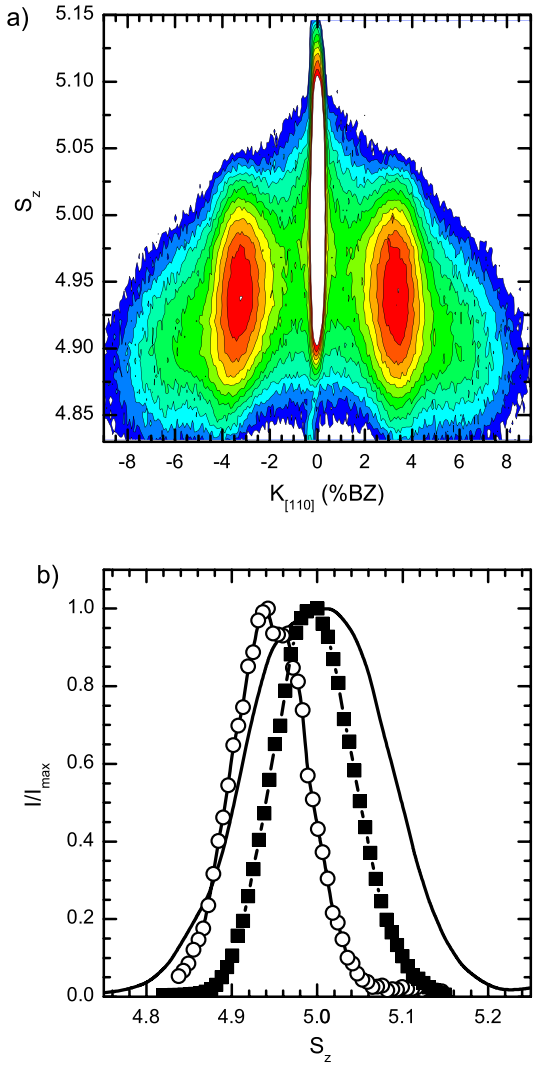

Figure 3. (a) Contour plot of the diffraction intensity as a function of the parallel and perpendicular wavevectors, $k_{//}$ and S_z, after sputtering along $[1\bar{1}0]$ for 2 h at 235 K. (b) Normalized intensity as a function of the perpendicular wavevector S_z after 0.5 ML of homoepitaxial growth on Cu(001) at 250 K (solid line), of the specular beam of the profile shown in (a) (filled squares) and for the side peak at 3.5% BZ (circles).

specular beam. Various ion fluxes were used in the experiments shown. We found that for an ion flux of 1.5×10^{16} ions m^{-2} s^{-1} the FWHM of the specular beam was always around $\Delta S_z = 0.10$. For an ion flux of 6×10^{16} ions m^{-2} s^{-1}, as used by van Dijken *et al* [15, 16], we found a similar value for sputter times up to 1 h. Extended sputtering led however to a smaller FWHM, indicating that the higher flux resulted in structures in which gradually more layers are involved.

Grazing incidence sputtering along the [100] azimuth also results in a diffraction pattern characteristic for nanogrooves; see the right panel of figure 2. Energy dependent line scans along [010] confirmed that the observed features indeed reflect the periodicity of a nanogroove pattern, although with a slightly larger average separation distance. The first order diffraction feature is considerably broader compared to the result obtained after sputtering along the high symmetry

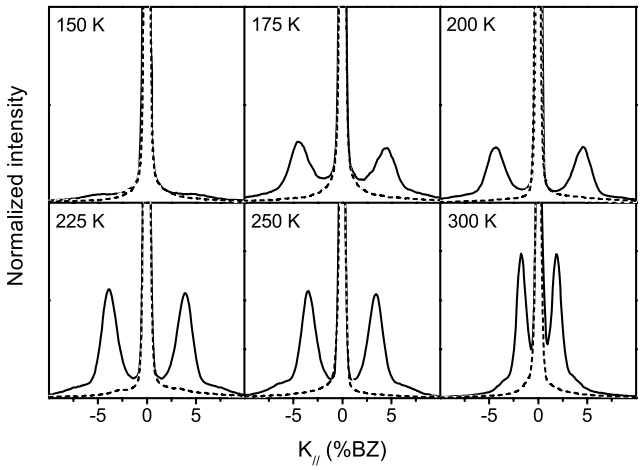

Figure 4. HR-LEED line scans through the specular beam acquired after 800 eV Ar ion sputtering at 80° in the $[1\bar{1}0]$ direction and at the substrate temperatures indicated. The incident ion flux was 1.5×10^{16} ions m^{-2} s^{-1} and the sputter time 1 h. The dashed and solid line scans were measured in the plane of incidence and the perpendicular direction respectively, and obtained at $E = 280$ eV. ($S_z = 4.94$.)

$[1\bar{1}0]$ azimuth, which also results in a lower intensity of the diffraction features depicted in figure 2, which were recorded under similar diffraction conditions.

4. Influence of substrate temperature

The well ordered nanogroove structure evolves in a wide temperature range for grazing incidence ion beam erosion. This is illustrated by the HR-LEED measurements in figure 4. The dashed and solid lines through the specular beam are measured in the plane of incidence and the perpendicular direction respectively and the intensity is normalized to the intensity of the in-phase Bragg peak at $S_z = 5$. For substrate temperatures between 175 and 300 K, the spot profiles show well developed peaks perpendicular to the plane of incidence of the Ar^+-ion beam, while no distinct diffraction features are measured parallel to this plane. As outlined earlier, these spot profiles must be interpreted as resulting from ion sputtering induced nanogroove structures with the lines oriented parallel to the plane of incidence. Van Dijken *et al* [15, 16] found that the width of the diffraction feature versus its position is constant, i.e. the line scans coincide with each other if the parallel electron wavevector and intensity are multiplied by appropriate numbers. This scaling behaviour indicates that the ratio σ/L of the Gamma distribution does not depend on temperature and points to a kinetic origin of the processes involved in the formation of the nanogroove pattern. A thermodynamic origin of the nanogrooves would be related to thermal fluctuations of steps that are very different over the broad temperature range considered. This would have led to strongly differing nanogroove separation distributions as a function of temperature [29]. We observed this scaling behaviour for ion sputtering along both azimuths with $\sigma/L = 0.5$ for sputtering along the [110] azimuth.

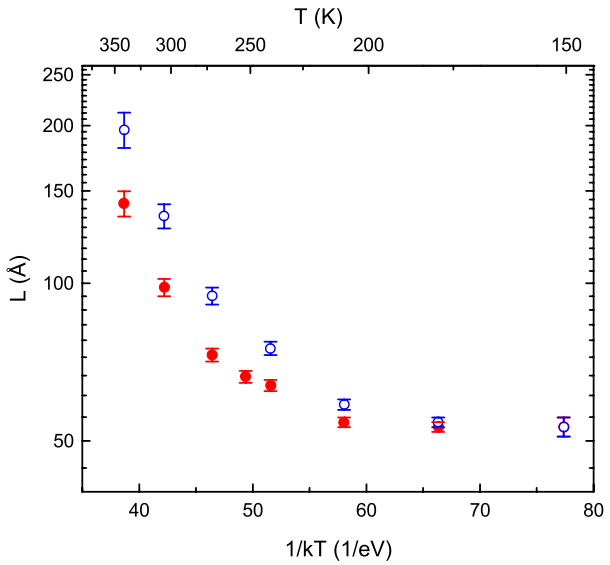

Figure 5. Average nanogroove separation as a function of the sputtering temperature after one hour of Ar^+-ion sputtering in the $[1\bar{1}0]$ (filled circles) or [100]-direction (open circles). A polar angle of incidence of 80° and an ion current of $\Phi = 5 \times 10^{12}$ ions cm^{-2} s^{-1}.

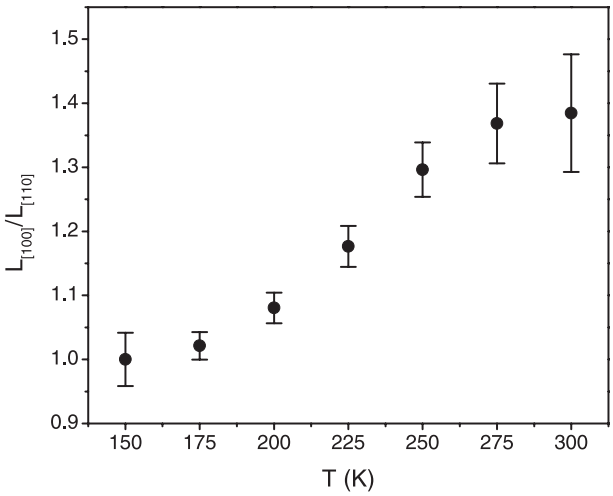

Figure 6. Nanogroove separation ratio L_{100}/L_{110} as a function of sputtering temperature as determined from the average nanogroove separation depicted in figure 5.

From the HR-LEED measurements in figure 4 and many others, the average nanogroove separation L as a function of the sputtering temperature was determined. The temperature dependence of L for sputtering along either the $[1\bar{1}0]$ or [100] azimuth is shown in figure 5. Sputtering along either azimuth leads to a similar temperature dependence of the average nanogroove separation. At substrate temperatures above 200 K, the average separation between nanogrooves increases with increasing temperature. In the case of homoepitaxial growth, the slope in the L versus $1/T$ plot can be used to determine the activation energy for adatom diffusion on flat terraces. For several reasons it is too ambiguous to extract an activation energy from the slope in figure 5. First of all, several different species like monovacancies, adatoms and larger vacancy and adatom islands are created during ion sputtering. The adatoms will diffuse over the surface until they meet others to form a stable adatom island or they recombine with vacancies. In both cases, adatoms influence the lateral length scale of the growing film. The direct creation of larger vacancy islands increases the density of stable vacancy islands. As a consequence, the energy tentatively obtained from the slope in figure 5 deviates considerably from the activation energy of for instance a monovacancy diffusion on a flat terraces when direct creation of larger vacancy islands is efficient.

At substrate temperatures below 200 K, the average separation between nanogrooves is not temperature dependent anymore (see figure 5). The minimum line separation is about 54 Å (21 atomic distances), which is considerably larger than the minimum separation between adatom islands measured after homoepitaxial growth (≈26 Å [30]). In the low temperature range, the energy transfer as a result of the ion impact plays a prominent role for the value of the average separation distance. This was illustrated by the linear dependence between average nanogroove separation and ion energy for grazing incidence sputtering of a Cu(001) substrate at low temperature [16]. This linear relation was found over an extensive energy range and independent of the mass of the ion used. The energy transfer upon ion impact results in a locally enhanced vibrational excitation exactly around the position of ion impact and enables diffusion processes until the transferred energy is relieved again. Especially detachment of either adatoms or vacancies that form the first step in the rearrangement of atoms on the surface is enabled at these low temperatures. These detachment processes have a considerable activation energy barrier (0.89 eV [31]) and would without the presence of the ion beam not occur at any appreciable rate. This also explains why these nanogroove patterns are stable for many hours up to temperatures of 230 K.

A marked difference between sputtering along either the $[1\bar{1}0]$ or the [100] azimuth is that the average nanogroove separation is substantially larger for the [100] azimuth for temperatures above 200 K. This difference is highlighted by the ratio depicted in figure 6. Around 150 K, when all thermally activated processes are frozen, the average nanogroove separation is similar. With increasing temperature the difference increases. This temperature dependence points to the role of thermally activated diffusion processes as the origin for this difference, as the result of the ion impact itself is virtually temperature independent.

5. Temporal evolution of the nanogroove pattern

A scenario for the creation of the regular array of shallow grooves was presented by Van Dijken *et al* [15, 16]. In the first stage, the major part of the grazing incident ions is specularly reflected by the surface without any change in morphology. The reflection occurs through a gradual change in path direction whilst the ion skims over the surface for several atomic distances before leaving the near surface region. The Cu surface atoms are as a result of thermal fluctuations at

slightly different positions away from their average positions. The ion observes these fluctuations as a snapshot, i.e. a frozen, slightly corrugated surface, and inelastic ion surface collisions become possible [32], leading to the creation of both isolated vacancies and adatoms, as well as atoms injected in the vacuum [33, 34]. The bulk vacancies will be much closer to the surface compared to the situation at normal incidence. Adatoms created through the same impact, or diffusing around after being generated previously, may annihilate the freshly produced monovacancy and part of the vacancy islands. This will result in 1 ML deep square vacancy islands with steps preferentially oriented along a ⟨110⟩ azimuth. This result is similar to submonolayer normal incidence sputtering on Cu(001), although the creation rate of vacancy islands is smaller for grazing incidence sputtering.

In phase two, the grazing incident ion approaches a previously created vacancy island. The ascending step of this vacancy island in the direction of the ion beam is a comparatively large target and receives a relatively high flux for geometric reasons. A much larger sputter yield of the ascending step compared to the terrace at grazing incidence was shown for Pt(111) [23] and Cu(001) [35]. An ion impact on the ascending step of a vacancy island results in an anisotropic enlargement in the direction of the ion beam.

In phase three a preferential coalescence of vacancy structures parallel to the plane of incidence occurs. Immediately after coalescence the edges of the merged clusters are smoothened efficiently for two reasons. First, the edges of the nanogrooves are smoothened by the continuously incoming ions as protruding illuminated kink atoms are eroded with high preference. Second, thermodynamics tends to reduce a high density of kinks, facilitated by the high mobility of adatoms along ⟨110⟩ steps on the fcc(001) surface.

The temporal evolution of the nanogroove pattern is illustrated in figure 7 for sputtering along either the [1$\bar{1}$0] or the [100] azimuth. An ion flux of 1.5×10^{12} ions cm^{-2} s^{-1} was used in these experiments. For this incident flux, the height of the nanogrooves is two atomic levels high, i.e. independent of sputter time. This temporal behaviour adds a fourth stage to the scenario, in which an increase of the average nanogroove separation occurs. This fourth stage is the only stage that can be observed with low energy electron diffraction. The density of structures in the first phases was found to be not large enough to give a reasonable diffraction signal. We do not expect a sharp distinction between the various phases and they will overlap in time while they occur on various places on the surface. Their distinction stems from the various active processes. Several distinctive similarities and differences were observed from time dependent sputter experiments over a wide temperature region.

(i) The average nanogroove separation of the nanogroove pattern increases with ion fluence and the rate of increase is strongly temperature dependent. An increase of about 10% after 4 h sputtering is found for temperatures below 200 K, while at temperatures of 300 K and above it amounts to at least 50%. The resolution of the HR-LEED system actually limits the determination of the average nanogroove separation to 40 nm, a value observed for sputtering for 2 h at 320 K along the [1$\bar{1}$0] azimuth.

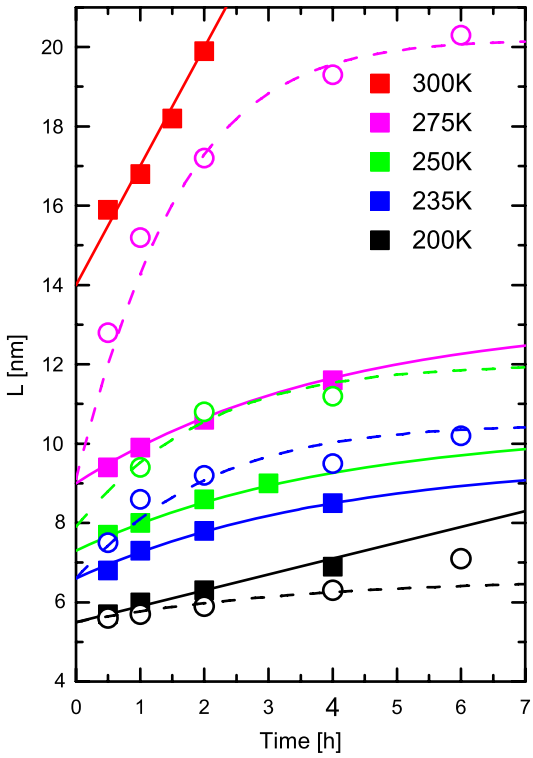

Figure 7. Average nanogroove separation as a function of sputter time for sputtering along the [1$\bar{1}$0] (solid squares) and [100] (circles). Measurements for the temperatures indicated are shown. A polar angle of incidence of 80° and an ion current of $\Phi = 1.5 \times 10^{12}$ ions cm^{-2} s^{-1} were used. The lines represent a fit according to equation (2) for sputtering along the [1$\bar{1}$0] azimuth (solid line) and for sputtering along the [100] azimuth (dashed line).

(ii) A saturation of the average nanogroove separation L is observed for sputtering along the [100] azimuth within 6 h. A more linear increase with time is observed for sputtering along the [1$\bar{1}$0] azimuth and even a four times larger sputter time (not shown) only indicated a slower increase.

(iii) A linear extrapolation to the start of the ion bombardment gives a similar starting separation distance for bombarding along either the [1$\bar{1}$0] or the [100] azimuth at a specific temperature. This similar distance agrees well with the formation of isotropic vacancy islands in the initial stage of the scenario sketched above. The mechanisms involved in the later phases lead to an azimuth dependent temporal behaviour. The ratio of the average nanogroove separation as shown in figure 6 is related to a snapshot of this movement after 1 h sputtering. Around 150 K, thermally activated diffusion processes are of no consequence on the timescale considered and the 'thermal spike' caused by the ion impact facilitates the local ordering.

(iv) The line scans displaying the periodicity after sputtering along the [1$\bar{1}$0] azimuth, measured for various temperatures shown in figure 2, scale with respect to each other. The diffraction line scans obtained for sputtering along the [100] azimuth, recorded after various ion bombardment times, also scale with respect to each other. This indicates

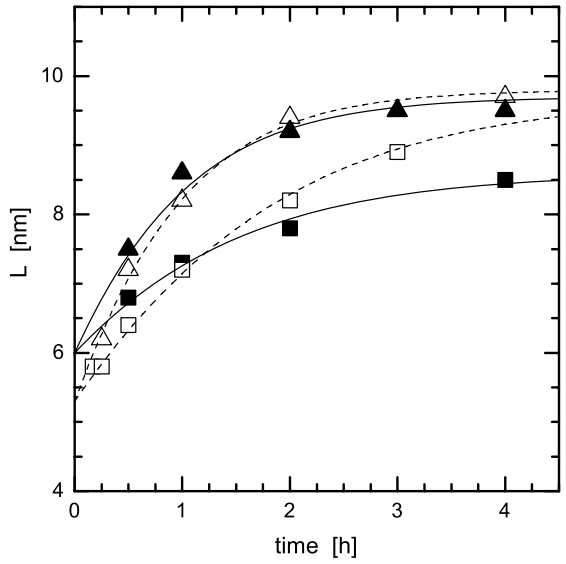

Figure 8. Distance between nanogrooves L as a function of sputter time at a substrate temperature of 235 K for a flux of 1.5×10^{16} ions m^{-2} s^{-1} (filled symbols) and 5×10^{16} ions m^{-2} s^{-1} (open symbols). The sputtering is along [1$\bar{1}$0] (square symbols) or [100] (triangle symbols). The lines are the fits according to equation (2).

that also the saturation of the average nanogroove separation is determined by kinetic effects rather than thermodynamics.

Increasing the flux to 5×10^{16} ions m^{-2} s^{-1} resulted in diffraction patterns similar to the one shown in figure 8. However, as mentioned before, the electron energy dependent line scans show that the height of these structures gradually increases with sputter time. After 1 h sputtering only three layers are involved in the height distribution. With increasing sputter time we find structures with four layers involved and finally structures with five layers involved. The increase with time of the average nanogroove separation for sputtering along the [1$\bar{1}$0] azimuth is distinctively higher for the higher ion flux, see figure 8. On the other hand, hardly any difference is found in the time evolution for sputtering, with a four times higher flux along the [100] azimuth. The apparent saturation of the average nanogroove separation is very similar for both sputter ion currents. A marked difference for both azimuths is the initial behaviour. The higher flux results in a lower value of the cut-off separation distance for extrapolating to zero time. This observation is in line with nucleation rate theory [36]. Equivalent to growth, the higher flux leads to a larger density of adatom, respectively vacancy, islands. A larger number of vacancy islands is expected to induce a smaller initial average separation distance. This feature reconfirms the nucleation part of the scenario. This result for two different ion fluxes also shows that for this system the average nanogroove separation does not scale with the ion dose, irrespective of the ion flux.

6. Annealing of nanogrooves

The formation of the nanogrooves is a subtle interplay between the sequential ion impacts and (an)isotropic diffusion processes

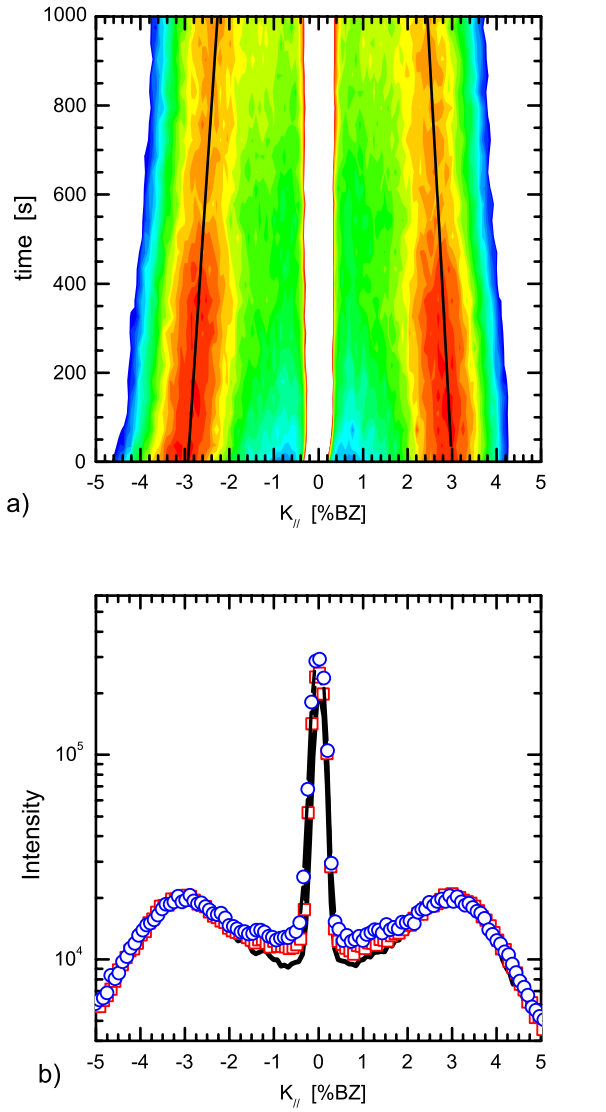

Figure 9. (a) Sequentially recorded 1D line scans along [010] and with $K_{[100]} = 0$ during annealing at 250 K of nanogrooves created after 1 h low flux sputtering at 235 K with the ion beam incident along [100]. In order to enhance the diffraction features of the nanogrooves, the specularly reflected beam is cut off and shows up as the central white area. (b) 1D line scans at the start of the annealing (solid line) and after 175 s (red squares) and 350 s (blue circles) annealing. The wavevectors of the line scans after 175 s and 350 s are scaled along [010], i.e. expanded by factors of 1.06 and 1.1, respectively.

on the surface. The influence of the diffusion mechanism can be isolated by observing the behaviour of the nanogroove pattern in the absence of the ion beam, i.e. observing the change in morphology during annealing. The annealing study starts with the preparation of a nanogroove pattern along either the [1$\bar{1}$0] or [100] azimuth for 1 h at 235 K. Subsequently, diffraction profiles were recorded while annealing the substrate at 250, 275 or 290 K. Figure 9(a) shows a contour plot of 1D line scans along the [010] azimuth during annealing at 250 K for nanogrooves created by sputtering along the [100] azimuth. An increase of the specularly reflected intensity is observed (not shown) that indicates an overall smoothening of

the surface. Annealing for a substantial time (over 10 min for ripples oriented along [100] at this temperature) also results in a gradual deterioration of the nanogroove structure as noticed by the decrease in intensity of the diffraction side peaks. Before this, the decrease of the diffraction features is hardly noticeable and the only marked change is the change in the average nanogroove separation L. Figure 9(b) shows the diffraction profile before the annealing started and after annealing for 175 and 350 s. The parallel component of the wavevector k of the scattered electrons in the measurements of the annealed substrate were multiplied by 1.06 and 1.10 for these two times, respectively. The very similar diffraction profiles show that the line scans scale with respect to each other. The ratio of the width of the distribution and the average distance between the nanogrooves is not altered by the annealing process. Note that a small deterioration in the first stage of the first line scan can be observed in figure 9(a) as the sample temperature is increased from 100 to 250 K. This temperature change affects the sample alignment and thus influences the parallel wavevector. In subsequent line scans, the sample alignment is corrected automatically by the HR-LEED software [37]. An approximately linear increase with time of the average periodicity L is observed in figure 9 with $\mathrm{d}L/\mathrm{d}t = 7\ \mathrm{nm\,h^{-1}}$. This increase of the nanogroove periodicity is significantly larger than observed during ion erosion, which amounts to $\mathrm{d}L/\mathrm{d}t = 2.4\ \mathrm{nm\,h^{-1}}$ at this temperature. The ion sputtering process is thus not essential for the increase of the periodicity L with time. Moreover, the annealing experiment shows that sputtering even slows down the temporal behaviour.

The annealing of the nanogrooves created by sputtering for 1 h at 235 K along $[1\bar{1}0]$ shows a similar linear increase of L with time. During annealing at 250 K, nanogrooves show an increase in periodicity with time of 4.7 $\mathrm{nm\,h^{-1}}$. This is a substantially lower value than the increase with time of 7 $\mathrm{nm\,h^{-1}}$ noted for nanogrooves created by sputtering along the [100] azimuth. We also noted that the nanogrooves created by sputtering along the $[1\bar{1}0]$ azimuth are much more anneal resistant.

7. Discussion

The experiments presented above provide insight into the temporal evolution of the nanogrooves. This is an extension of the initial work of Van Dijken *et al* [15, 16], who limited their study to nanogrooves obtained after sputtering for 1 h at different temperatures. Their deconvoluted diffraction profiles were shown to scale to each other; i.e., the distribution of the nanogroove separation is independent of temperature. This conservation property indicates that the process underlying the setting of the periodicity L is kinetic in origin. In this manuscript, it was shown that the diffraction profiles recorded under a variety of circumstances (fluence, flux, temperature and annealing) showed a similar ratio of width of the distribution to the average nanogroove separation distance. Sputtering along the [100] azimuth results only in a slightly larger ratio. The scaling behaviour therefore includes those line scans taken after 4 h sputtering along the [100] azimuth, i.e. in the regime where we observed clear saturation behaviour for the average nanogroove separation. The saturation itself is thus part of the kinetics.

The kinetics of ion induced ripples on Cu(001) was also studied experimentally by Chason and co-workers [9, 38]. They concluded that their ripple structure has the features of a Bradley–Harper instability. Their ripples were created by 800 eV Ar^+ sputtering at 70° angle of incident with the normal in the temperature range of 415–455 K and for ion fluxes of 10^{18} ions $\mathrm{m^{-2}\ s^{-1}}$ and similar sputter times. Although it would be tempting to make a direct comparison of their results and the results presented in this work, they are markedly different. This difference is illustrated by comparing the results for 70° and 80° ion erosion on Ag(001) for temperatures above 300 K [20]. In the present work, ion erosion at an angle of 80° leads to the formation of shallow nanogrooves. A variation of the polar angle of incidence leads to a very different morphology for non-grazing incidence ion erosion. This is due to the fact that a total reflection of the ion beam occurs for grazing incidence, leading to a sharp reduction in sputter yield. The critical angle for this grazing incidence is around a polar angle of 75° [22]. As already appreciated by Bradley and Harper [2], the different sputter mechanisms at grazing incidence make their continuum description inapplicable for this situation. The second reason for the difference is displayed in the kinetic phase diagram that was published for sputtering of Cu and Ag(001) surfaces [10]. This diagram relates the high temperature measurements by Chason *et al* to a regime characterized by BH instabilities, while our present measurements are in a regime that is dominated by Ehrlich–Schwoebel (ES) instabilities.

The continuum approach of Bradley and Harper has been modified to incorporate many additional processes compared to the original Sigmund ion impact and Mullins diffusion description. These approaches generally predict critical exponents that describe the time evolution of the roughness and characteristic length scale on the surface. Such critical exponents can be derived for sputtering along the $[1\bar{1}0]$ azimuth. This approach fails to describe the temporal evolution for sputtering along the [100] azimuth; it is unable to describe the saturation behaviour. Moreover, Aste and Valbusa [17] showed that a continuum description that incorporates anisotropic diffusion as a result of ES barriers predicts a behaviour different from the observations in this work. Their analysis showed that an increase in ripple periodicity is accompanied by an exponential growth of the roughness of a ripple pattern. Grazing incidence sputtering of Cu(001) with a flux of 1.5×10^{12} ions $\mathrm{cm^{-2}\ s^{-1}}$ does not lead to any noticeable increase in roughness, while the average nanogroove separation increases up to 50%. This behaviour is very different from the ripple formation on Cu(110) investigated by Rusponi *et al* [13] in the same temperature regime, but at a smaller polar angle of incidence. Their ripple structures obtained after sputtering at grazing incidence of 45° or 70° (from the surface normal) showed an increase in both ripple periodicity and roughness.

The annealing behaviour of the nanogroove pattern provides information regarding the diffusion processes active on the surface. We observe a quite linear increase in

the average nanogroove separation, while the distribution remains similar. This behaviour cannot be understood from the Mullins description of diffusion. First of all a clear diffusion anisotropy is observed, which explains the larger average nanogroove separation observed after 1 h sputtering along the [100] azimuth compared to the [1$\bar{1}$0] azimuth. Moreover, the isotropic Mullins diffusion that is used in the BH model predicts a $t^{1/4}$ change in average nanogroove separation. The measurements show an increase of average nanogroove separation with time that has to be described with an exponent of at least 0.75, while an exponent of 1 gives an excellent representation. We therefore start by presenting a different description of the influence of diffusion on the average nanogroove separation. The observed increase of L during annealing and the scaling of the line scans implies that nanogrooves with a small average size have disintegrated and their mass has been redistributed leading to nanogrooves with an on average larger separation distance. This implies a massive mass transport across the surface and also that the surviving nanogrooves themselves move across the surface. Such mass transport in the absence of the ion beam is at these temperatures only possible due to the creation of both adatoms that traverse the terrace between the nanogrooves as well as through vacancy creation and subsequent diffusion through the high(er) level(s) of nanogrooves. The impact of vacancies in mass transport on Cu(001) was suggested by Hannon *et al* [39] and several STM experiments have shown the influence of vacancies created at steps [40–42]. The activation barrier for diffusion of vacancies and adatoms on Cu(001) is very similar (about 0.44 eV [39, 43]). Both were determined simultaneously in a recent experimental study on the initial phase of normal incidence sputtering [35]. The influence of both adatoms and vacancy diffusion on stepped surfaces was considered theoretically by Hare and Roelofs [44]. Their results are not applicable in this case as a terrace on a vicinal surface is bound by both an ascending and a descending step. A lower terrace on a nanogrooved surface is however, bound by two ascending steps.

The motion of the nanogrooves will be first discussed in the absence of the ion beam. The creation of adatoms on the lower terrace between two nanogrooves starts with a thermally activated detachment process from one of the edges that bound the nanogroove. The detachment of an adatom from a step edge is a process that requires a relatively high energy compared to diffusion on the terrace of Cu(001) [31]. After the detachment of an adatom, its movement on the terrace itself is a random walk. The relatively high detachment energy (0.89 eV for a ⟨110⟩ step edge) compared to the diffusion energy (0.44 eV) implies that there is a low density of adatoms and vacancies on the surface. Nucleation of an adatom or vacancy island is unlikely. The frequency of detachment processes is determined by the kink density at the edges of the nanogrooves. Along a ⟨100⟩ azimuth, each atom at the step edge is bonded to the terrace by two nearest neighbour atoms. This provides a much higher kink density compared to a step edge along the ⟨110⟩ azimuth. In this case the step edge atom is generally bonded by three nearest neighbours, except for atoms at kinks, leading to a substantially smaller kink density. The high kink density is directly reflected in the higher thermally induced increase in the average separation distance observed for nanogrooves parallel to a ⟨100⟩ azimuth. The specific orientation of the step edge also explains the more rapid smoothening of nanogrooves created along ⟨100⟩. The interlayer mass transport is much larger over this step edge compared to ⟨110⟩ step edges [24, 45]. The actual height of the Ehrlich Schwoebel barrier that determines the interlayer mass transport was recently determined to be about nil for the ⟨100⟩ step edge and at least 0.12 eV for the ⟨110⟩ step edge [46]. Not only adatoms will traverse over the lower terrace of the nanogroove. Also vacancies will be created at the step edges of the nanogroove and these vacancies will traverse through the higher terrace of the nanogroove in a similar fashion as adatoms traverse over the lower terrace.

The observed annealing behaviour allows us to propose a model that describes the temporal behaviour of the nanogrooves. The change in the average nanogroove separation increases linearly with time. The creation of a new nanogroove between two already existing nanogrooves will depend on the distance between these two grooves. If they are far apart, a new groove can easily be made, while if they are quite close the groove will be annihilated by the already existing grooves. This leads to the following balance:

$$\frac{\mathrm{d}L}{\mathrm{d}t} = D - CL. \tag{1}$$

In this D describes the diffusion behaviour and C describes the probability for creating a new nanogroove. A stationary situation occurs when $D = CL$, i.e. when the distance between nanogrooves has become on average so large that further separation is compensated by the creation of new nanogrooves. This is a competition between two kinetic processes and thus leads to the observed scaling behaviour of the diffraction features even at the saturation length $\overline{L} = D/C$. The above model leads to a temporal dependence of L according to

$$L(t) = \frac{D}{C} + \mathrm{e}^{-Ct}\left(L_0 - \frac{D}{C}\right). \tag{2}$$

This relation can be used to describe the data at various temperatures; see figure 7. For sputtering along a ⟨100⟩ azimuth, the deviation from a linear increase with time allows us to obtain fairly accurate values for the three parameters. For sputtering along the [1$\bar{1}$0] azimuth only the temporal evolution at 275 K shows at first glance a marked deviation from a linear increase of the line separation. For 300 K, the linear increase suggests that the sputter time is below the characteristic nanogroove creation time $1/C$. In this case, $L(t) = L_0 + (D - CL_0)t$ and D and C cannot be determined independently. For the data recorded at 250 and 235 K a slight deviation from the linear increase can be observed and equation (2) can be used. For the high flux, also an apparent saturation can be observed sputtering along the [1$\bar{1}$0] azimuth. The fit to the nanogroove average separation recorded at 235 K for both the high and low flux is depicted in figure 8. A good description of the temporal evolution of L is found for all temperatures measured. At 250 K, D was found to

be 9 nm h^{-1}, quite close to the value found for annealing, 7 nm h^{-1}. The close correspondence of these numbers supports the assumption in our model that ions are not crucial for the increase in average nanogroove separation with fluence as observed. From this equation, one would expect a marked influence of the ion flux, i.e. a smaller saturation length scale for a higher flux. We do not observe this effect, which indicates that the creation of a new nanogroove is not linearly dependent on the ion flux. The influence of the ion beam for grazing incidence sputtering is not only to facilitate the creation of new nanogrooves, but it also plays a vital part in the shaping of the nanogrooves. Irregularities in the nanogroove edges are high impact positions for grazing incidence sputtering. As such, the detachment kinetics that determine the diffusion behaviour will be enhanced by the presence of an ion beam and would also explain the faster increase in average separation distance as we observed for a higher flux sputtering along the ⟨110⟩ azimuth; see figure 8.

8. Conclusion

Grazing incidence sputtering enables the creation of very shallow (two atomic layers deep) 1D nanostructures on Cu(001) with an average nanogroove separation that can be set by controlling the sputter time and temperature, between 5 and 35 nm. The processes on an atomic scale that are responsible for the creation of these nanogrooves and the change in average nanogroove separation with prolonged sputtering have been identified. The scenario initially proposed by Van Dijken *et al* [15, 16] for the creation of these nanogrooves is supported by the azimuth independent distance between initially created vacancy islands. In further sputtering, the specific azimuth along which the ion beam is aligned determines the rate at which the average separation of the nanogrooves changes. This is a direct consequence of the crystalline nature of the substrate surface. The orientations of step edges provide a difference in kink density. The detachment from a kink position is the rate limiting step for the change in the average nanogroove separation. Moreover, at grazing incidence ions have very different sputter probabilities on flat terraces and for small protrusions. These small protrusions in the form of a step are preferentially removed. This effect leads to an excellent definition of the nanogroove pattern that counters smoothening diffusion processes. The diffusion of both vacancies and atoms is responsible for the increase in average nanogroove separation with time. In the absence of the ion beam this increase is very similar, but also the interface roughness decreases. The ion beam assures a constant creation of new starting points for nanogrooves and thus counterbalances the observed increase in average nanogroove separation. The ratio of the diffusion and the creation of new nanogrooves thus eventually leads to a balanced situation that is observed as a saturation of the average nanogroove separation of the nanogrooves.

Acknowledgments

This work is part of the research programme of the Stichting voor Fundamenteel Onderzoek der Materie (FOM), which is financially supported by the Nederlandse organisatie voor Wetenschappelijk Onderzoek (NWO). The authors acknowledge the contributions of Sebastiaan van Dijken, Mischa Ovsyanko and Georgiana Stoian to this work.

References

[1] Navez M, Sella C and Chapertot D 1962 Microscopie electronique-étude de lattaque du verepar bombardement ionique *C. R. Acad. Sci. Paris* **254** 240
[2] Bradley R M and Harper J M E 1988 Theory of ripple topography induced by ion bombardment *J. Vac. Sci. Technol.* A **6** 2390
[3] Sigmund P 1973 A mechanism of surface micro-roughening by ion bombardment *J. Mater. Sci.* **73** 1545
[4] Mullins W W 1957 Theory of thermal grooving *J. Appl. Phys.* **28** 333–9
[5] Mullins W W 1959 Flattening of a nearly plane solid surface due to capillarity *J. Appl. Phys.* **30** 77–83
[6] Park S, Kahng B, Jeong H and Barabási A L 1999 Dynamics of ripple formation in sputter erosion: nonlinear phenomena *Phys. Rev. Lett.* **83** 3486
[7] Cuerno R and Barabási A L 1995 Dynamic scaling of ion-sputtered surfaces *Phys. Rev. Lett.* **74** 4746
[8] Makeev M A, Cuerno R and Barabási A L 2002 Morphology of ion-sputtered surfaces *Nucl. Instrum. Methods Phys. Res.* B **197** 185
[9] Chan W L, Pavenayotin N and Chason E 2004 Kinetics of ion-induced ripple formation on Cu(001) surfaces *Phys. Rev.* B **69** 245413
[10] Chan W L and Chason E 2007 Making waves: kinetic processes controlling surface evolution during low energy ion sputtering *J. Appl. Phys.* **101** 121301
[11] Rusponi S, Boragno C and Valbusa U 1997 Ripple structure on Ag(110) surface induced by ion sputtering *Phys. Rev. Lett.* **78** 2795
[12] Rusponi S, Costantini G, Boragno C and Valbusa U 1998 Ripple wavevector rotation in anisotropic crystal sputtering *Phys. Rev. Lett.* **81** 2735
[13] Rusponi S, Costantini G, Boragno C and Valbusa U 1998 Scaling laws of the ripple morphology on Cu(110) *Phys. Rev. Lett.* **81** 4184
[14] Valbusa U, Boragno C and de Mongeot F B 2002 Nanostructuring surfaces by ion sputtering *J. Phys.: Condens. Matter* **14** 8153–75
[15] van Dijken S 2000 Pattern formation and magnetic anisotropy in thin metal films *PhD Thesis* University of Twente ISBN 90-365-1459-2
[16] van Dijken S, de Bruin D and Poelsema B 2001 Kinetic physical etching for versatile novel design of well ordered self-affine nanogrooves *Phys. Rev. Lett.* **86** 4608–11
[17] Aste T and Valbusa U 2005 Ripples and ripples: from sandy deserts to ion-sputtered surfaces *New J. Phys.* **7** 122
[18] Pedemonte L, Braco G, Boragno C, Buatier de Mongeot F and Valbusa U 2003 Smoothing of nanoscale surface ripples studied by He atom scattering *Phys. Rev.* B **68** 115431
[19] Kim T C, Ghim C M, Kim H J, Kim D H, Noh D Y, Kim N D, Chung J W, Yang J S, Chang Y J, Noh T W, Kahng B and Kim J S 2004 Kinetic roughening of ion-sputtered Pd(001) surface: beyond the Kuramoto–Sivashinsky model *Phys. Rev. Lett.* **92** 246104
[20] Everts F, Wormeester H and Poelsema B 2008 Optical anisotropy induced by ion bombardment of Ag(001) *Phys. Rev.* B **78** 155419
[21] Munoz-Garcia J, Castro M and Cuerno R 2006 Nonlinear ripple dynamics on amorphous surfaces patterned by ion beam sputtering *Phys. Rev. Lett.* **96** 086101

[22] Niehus H, Heiland W and Taglauer E 1993 Low-energy ion scattering at surfaces *Surf. Sci. Rep.* **17** 213
[23] Hansen H, Polop C, Michely M, Friedrich A and Urbassek H M 2004 Step edge sputtering yield at grazing incidence ion bombardment *Phys. Rev. Lett.* **92** 246106
[24] Broekmann P, Mewe A A, Wormeester H and Poelsema B 2002 Step edge selection during ion erosion of Cu(001) *Phys. Rev. Lett.* **89** 146102
[25] Wollschläger J 1997 Simple analysis of spot splitting due to diffraction at surfaces with atomic steps *Surf. Sci.* **383** 103
[26] Horn M, Gotter U and Henzler M 1988 Low-energy electron diffraction investigations of Si molecular-beam epitaxy onto Si(100) *J. Vac. Sci. Technol.* B **6** 727
[27] Altsinger R, Busch H, Horn M and Henzler M 1988 Nucleation and growth during molecular beam epitaxy (MBE) of Si on Si(111) *Surf. Sci.* **200** 235
[28] Furman I, Biham O, Zuo J-K, Swan A K and Wendelken J F 2000 Epitaxial growth of Cu on Cu(001): experiments and simulations *Phys. Rev.* B **62** R10649–52
[29] Williams E D and Bartelt N C 1991 Thermodynamics of surface morphology *Science* **251** 393
[30] Jorritsma L C, Bijnagte M, Rosenfeld G and Poelsema B 1997 Growth anisotropy and pattern formation in metal epitaxy *Phys. Rev. Lett.* **78** 911
[31] Biham O, Furman I, Karimi M, Vidali G, Kennett R and Zeng H 1998 Models for diffusion and island growth in metal monolayers *Surf. Sci.* **400** 29
[32] Poelsema B, Verhey L K and Boers A L 1976 Study of low energy noble gas ion reflection from monocrystalline surfaces; influence of thermal vibrations of the surface atoms. I. Computer simulation of energy and spatial distributions *Surf. Sci.* **55** 445–66
[33] Michely T and Teichert C 1994 Adatom yields, sputtering yields, and damage patterns of single-ion impacts on Pt(111) *Phys. Rev.* B **50** 11156
[34] Costantini G, de Mongeot F B, Boragno C and Valbusa U 2001 Is ion sputtering always a 'negative homoepitaxial deposition'? *Phys. Rev. Lett.* **86** 838
[35] Stoian F G 2008 Primary effects in ripple formation induced by erosion and growth of Cu(001) *PhD Thesis* University of Twente
[36] Venables J A 1973 Rate equation approaches to thin film nucleation kinetics *Phil. Mag.* **27** 697
[37] Esser M 2001 Kinetically controlled Si-epitaxy on Si(100) and Ge(100) *PhD Thesis* University of Twente ISBN 90-365-1641-2
[38] Shenoy V B, Ramasubramaniam A, Ramanarayan H, Tambe D T, Chan W L and Chason E 2004 Influence of step-edge barriers on the morphological relaxation of nanoscale ripples on crystal surfaces *Phys. Rev. Lett.* **92** 256101
[39] Hannon J B, Kluenker C, Giesen M, Ibach H, Bartelt N C and Hamilton J C 1997 Surface self-diffusion by vacancy motion: island ripening on Cu(001) *Phys. Rev. Lett.* **79** 2506
[40] Flores T, Junghans S and Wuttig M 1997 Atomic mechanism for the diffusion of Mn atoms incorporated in the Cu(001) surface: an STM study *Surf. Sci.* **371** 1–13
[41] Flores T, Junghans S and Wuttig M 1997 Atomic mechanism of the formation of an ordered surface alloy: an STM investigation of Mn/Cu(001) *Surf. Sci.* **371** 14–29
[42] van Gastel R, Somfai E, van Albada S B, Saarloos W and Frenken J W M 2002 Vacancy diffusion in the Cu(001) surface I: an STM study *Surf. Sci.* **521** 10–25
[43] Breeman M and Boerma D O 1992 Ion-beam induced generation of Cu adatoms on Cu(100) *Surf. Sci. Lett.* **278** 110
[44] Hare G and Roelofs L D 2002 Diffusion of vacancies and adatoms on stepped crystalline surfaces *Surf. Sci.* **511** 283–93
[45] Li M, Wendelken J F, Liu B G, Wang E G and Zhang Z 2001 Decay characteristics of surface mounds with contrasting interlayer mass transport channels *Phys. Rev. Lett.* **86** 2345
[46] Rabbering F L W 2008 On the interplay between steering and interlayer diffusion in Cu(001) homoepitaxy *PhD Thesis* University of Twente